

# Experiments on instability of thermocapillary convection in shallow annular liquid layers

**Shunichi Wakitani**

College of Industrial Technology, 1-27-1 Nishikoya, Amagasaki 661-0047, Japan

E-mail: wakitani@cit.sangitan.ac.jp

**Abstract.** Experimental study of thermocapillary convection of silicone oil (the Prandtl number  $Pr \approx 18$ ) was conducted in a shallow annular cavity with outer radius  $R_o = 55$  mm and inner radius  $R_i = 15$  or  $27.5$  mm for liquid heights  $H$  in the range 1–3 mm. The liquid layer is heated from the outer cylindrical wall and cooled at the inner wall. The experiments were performed over a wide range of Marangoni numbers,  $400 < Ma < 10000$ . The measurement of surface temperatures and observation of instability structures were made by using an IR thermography technique. As  $Ma$  exceeded a critical value, hydrothermal waves were observed for thin liquid layers,  $H \leq 2.5$  mm, of both the inner radii. These waves are characterized by curved spoke patterns propagating in the azimuthal direction. For thicker layers,  $H > 2.5$  mm, multicell patterns were dominant. At low  $Ma$ , the multicell patterns were steady, toroidal rolls. As  $Ma$  was increased, the rolls began to rotate around the centre and unsteady longitudinal rolls appeared. In the range  $2.5 \leq H \leq 2.8$  mm, hydrothermal waves and multicell coexisted. The transition map is presented in terms of  $Ma$  and  $Bo_a$ .

## 1. Introduction

Under a microgravity environment, the surface tension of an interface between two immiscible fluids is dominant in comparison with buoyancy force. The surface tension depends on temperature. Any temperature gradient may induce spatial gradients in surface tension and hence a fluid motion known as thermocapillary convection. For small geometry and/or microgravity environments, therefore, thermocapillary convection plays an important role in heat and mass transfer across interfaces.

In crystal growth processes by making use of floating-zone technique as well as Czochralski (CZ) technique, undesirable striations have often been observed. These striations may be attributed to oscillatory instability of the basic thermocapillary convection. Some experimental results of thermocapillary instabilities have been reviewed [1].

Smith and Davis [2] predicted the appearance of longitudinal rolls or oscillatory, hydrothermal waves according to the basic thermocapillary flow. In shallow, rectangular liquid layers, Riley and Neitzel [3] have first confirmed the appearance of oscillatory, hydrothermal waves. The transition from steady, unicellular convection to the oscillatory convection state is verified.

An annular liquid layer, the upper of which is the free surface, represents a model of the CZ crystal-growth process. Several experiments for shallow, annular configuration have already been made [4, 5]. Schwabe et al. [4] observed two different oscillatory instabilities, viz. a short wavelength instability, which propagated obliquely, for a shallow liquid layer and a long wavelength instability, which propagated radially around onset, for a deep layer. The former seems to correspond to a

hydrothermal wave, although some characteristics were different from those predicted by theory. The latter seems to relate to a surface-wave instability [6]. On the other hand, the instabilities observed by Ezersky et al. [5] were not due to pure hydrothermal waves [1]. Further, a few experiments have been reported under microgravity [7, 8].

Recently, a detail experiment has been made using shadowgraph method [9]. There, depending on the fluid depth, two types of hydrothermal waves have been observed. One is the hydrothermal wave (HW2) which propagates radially at onset for smaller fluid depth than a capillary length, the other (HW1) which propagates with an angle from radial direction for larger fluid depth. A proper experimental study may be needed to confirm their existence and behavior.

In this paper, thermocapillary convection of silicone oil in shallow annular layers is investigated over a wide range of parameters which characterize the flow using an IR thermography device. The following dimensionless parameters are used:

Prandtl number	$Pr = \nu / \kappa,$	aspect ratio	$Ar = (R_o - R_i) / H,$
Marangoni number	$Ma = \frac{\gamma \Delta T H^2}{\mu \kappa L},$	Rayleigh number	$Ra = \frac{g \beta \Delta T H^4}{\nu \kappa L},$
Bond number	$Bo = \frac{\rho g H^2}{\sigma},$	Dynamic Bond number	$Bo_d = Ra / Ma,$

where  $\nu$ ,  $\kappa$ ,  $\gamma$ ,  $\mu$ ,  $g$ ,  $\beta$ ,  $\rho$ ,  $\sigma$  are kinematic viscosity, thermal diffusivity, absolute value of temperature derivative of surface tension ( $= |\partial\sigma/\partial T|$ ), dynamic viscosity, acceleration due to gravity, thermal expansion coefficient, density and surface tension.  $R_o$  and  $R_i$  are the outer and inner radii of the annular layer,  $L = R_o - R_i$  is the gap length,  $H$  is liquid heights and  $\Delta T$  is the temperature difference between the outer and inner walls.

## 2. Experimental apparatus and method

Figure 1 shows a sketch of experimental apparatus. The experiments are conducted in a thin annular liquid layer of height  $H$ , and radius region  $R_i < r < R_o$ , where  $r$  indicates the radial coordinate system.

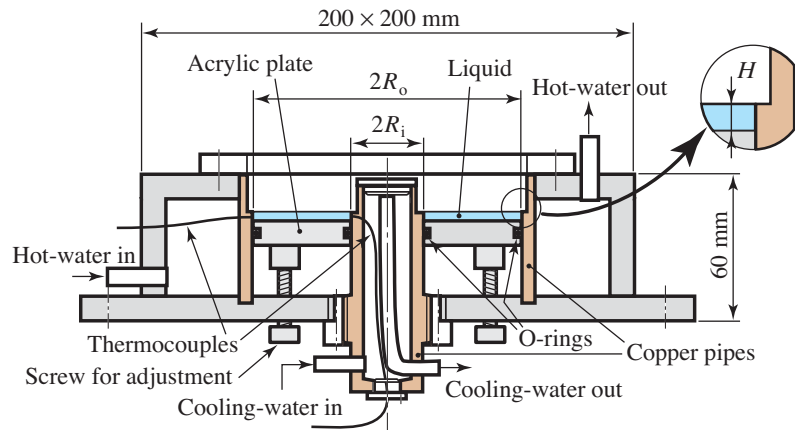


**Figure 1.** Experimental apparatus

As the working fluid a silicone oil (Dow corning Toray SH200-1cSt) was used with Prandtl number  $Pr \approx 18$ . Table 1 shows properties of the silicone oil used in this experiment.

Both inner and outer cylinders are made of copper 5 mm in thickness. In order to eliminate a meniscus and to obtain the flat interface, a 2 mm wide lip has been machined along the top of the edge of each cylinder wall and the free surface has been pinned at the edge [3]. With water temperature-

controlled from two constant-temperature baths the wall of the outer cylinder is heated to  $T_o$ , and the inner is cooled to  $T_i$ , thus temperature difference  $\Delta T = T_o - T_i$ . The temperatures at the outer and inner walls are measured using four T-type sheathed thermocouples and a sheathed thermocouple 1 mm in diameter, respectively.

**Table 1.** Physical properties of silicone oil (SH200-1cSt) (25°C)

density $\rho$	817 kg m <sup>-3</sup>
specific heat $c_p$	2047 J kg <sup>-1</sup> K <sup>-1</sup>
kinematic viscosity $\nu$	1.00 mm <sup>2</sup> s <sup>-1</sup>
thermal conductivity $k$	0.105 W m <sup>-1</sup> K <sup>-1</sup>
surface tension $\sigma$	17.4 mN m <sup>-1</sup>
temperature dependence of surface tension $\partial\sigma/\partial T$	-0.0755 mN m <sup>-1</sup> K <sup>-1</sup>
thermal expansion coefficient $\beta$	0.00134 K <sup>-1</sup>

The thermally insulating bottom is made of acrylic plate 10 mm in thickness. Liquid crystal thermal sensing sheet is attached on the bottom to make it possible to visualize simple temperature profiles, and the bottom is adjustable to a proper liquid height  $H$ . The experiments were conducted in the range  $1.0 \leq H \leq 3.0$  mm. The radius  $R_o = 55$  mm is fixed, but  $R_i = 15$  or 27.5 mm. Thus, the radius ratio ( $R_o/R_i$ ) is 3.7 or 2, the gap length  $L = R_o - R_i = 40$  or 27.5 mm, and aspect ratios are in the range  $9.2 \leq Ar \leq 40$ .

Transitions between various states were determined mainly using an IR thermography device (NEC SANEI TH9100MV).

### 3. Experimental results and discussion

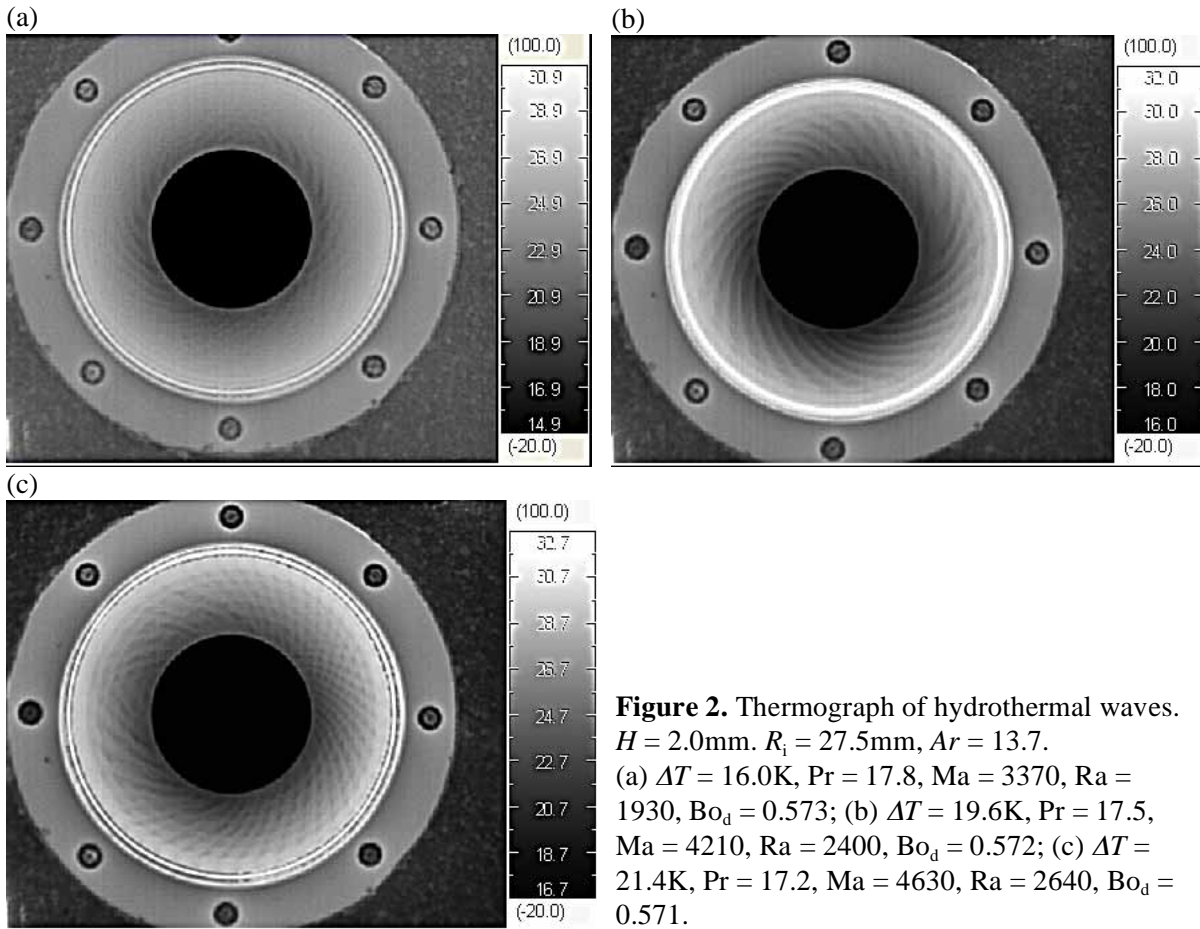
#### 3.1. Hydrothermal wave

As Marangoni number  $Ma$  exceeded a critical value, oscillatory instabilities corresponding to the hydrothermal waves were observed for thin liquid layers,  $H \leq 2.5$  mm ( $Bo_d \leq 0.9$ ), of both the inner radii  $R_i = 15$  and 27.5 mm. Although, for thicker layers,  $H > 2.5$  mm, multicell patterns described later were dominant, it was confirmed that weak hydrothermal waves still existed at  $H = 2.8$  mm ( $Bo_d = 1.1$ ). These hydrothermal waves were characterized by curved spoke patterns propagating in the azimuthal direction, owing to the surface basic flow toward the inner wall.

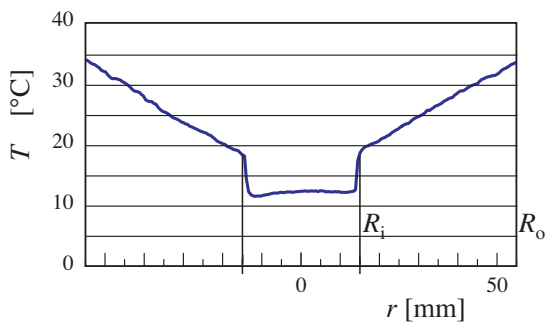
The waves which propagate in both azimuthal directions usually appear near onset. The intensities of these waves were different. Then, as  $Ma$  was increased, the grown waves began to propagate in an azimuthal direction. As  $Ma$  was further increased, the waves again propagated in two directions. Figure 2 shows examples of thermograph of such hydrothermal waves.

Figure 3 shows a surface temperature profile measured using an IR thermography camera. The surface temperature is almost linear in a liquid layer.

In careful experiments, we could not detect hydrothermal wave which propagates radially at onset (named as HW2 by [9]). However, as shown in figure 4, when the bottom of the cavity is not in horizontal plane, i.e. liquid height is not uniform, the hydrothermal waves which propagate radially appear obviously, in addition to the hydrothermal waves which propagate azimuthally. This figure is the case where liquid height  $H$  through the centerline varies linearly from 1 to 2 mm. In this case  $H$  is 1 mm at the downside edge of the outer wall and 2 mm at the upside edge in the figure. Some dimensionless parameters are estimated at  $H = 1.5$  mm. This result suggests that the occurrence of HW2 may be attributed to a locally non-uniform depth of liquid layers. The inner cylinder used in [9] seems to be finished in such a way that its edge becomes in same level as liquid surface to eliminate a meniscus without a lip. This method may give rise to undesirable disturbances near the inner wall.



**Figure 2.** Thermograph of hydrothermal waves.  $H = 2.0\text{mm}$ ,  $R_i = 27.5\text{mm}$ ,  $Ar = 13.7$ .  
 (a)  $\Delta T = 16.0\text{K}$ ,  $Pr = 17.8$ ,  $Ma = 3370$ ,  $Ra = 1930$ ,  $Bo_d = 0.573$ ; (b)  $\Delta T = 19.6\text{K}$ ,  $Pr = 17.5$ ,  $Ma = 4210$ ,  $Ra = 2400$ ,  $Bo_d = 0.572$ ; (c)  $\Delta T = 21.4\text{K}$ ,  $Pr = 17.2$ ,  $Ma = 4630$ ,  $Ra = 2640$ ,  $Bo_d = 0.571$ .



**Figure 3.** Surface temperature profile on central-cross section.  $H = 1.0\text{mm}$ ,  $R_i = 15\text{mm}$ ,  $\Delta T = 27.1\text{K}$ ,  $Pr = 16.8$ ,  $Ma = 1040$ ,  $Ra = 148$ ,  $Bo_d = 0.142$ .

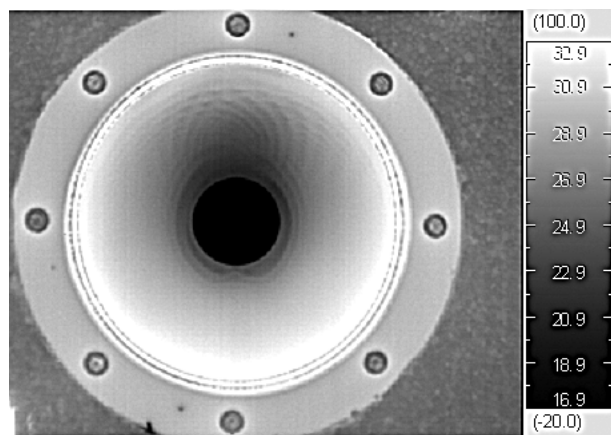


**Figure 4.** Thermograph of hydrothermal waves.  $R_i = 15\text{mm}$ ,  $H = 1\text{--}2\text{mm}$  ( $H = 1\text{mm}$  at downside edge of outer wall,  $2\text{mm}$  at upside edge in this figure),  $\Delta T = 23.2\text{K}$ ,  $Pr = 17.1$ ,  $Ma = 1960$ ,  $Ra = 629$ ,  $Bo_d = 0.321$ .

Figures 5 and 6 show propagation angle measured from radial direction, and wavelength of hydrothermal wave at central gap,  $(R_i + R_o)/2$ , respectively. Every angle is in the range 40–50 degrees. The wavelength seems to be roughly in proportion to liquid height.

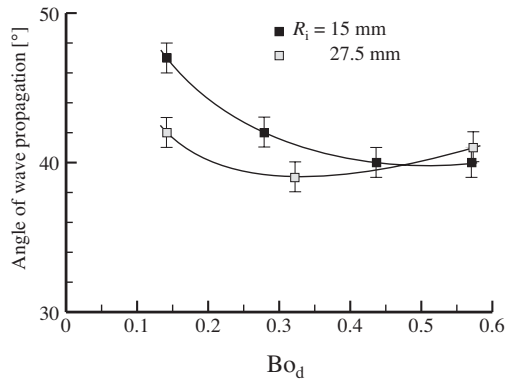


**Figure 5.** Propagation angle of hydrothermal wave.

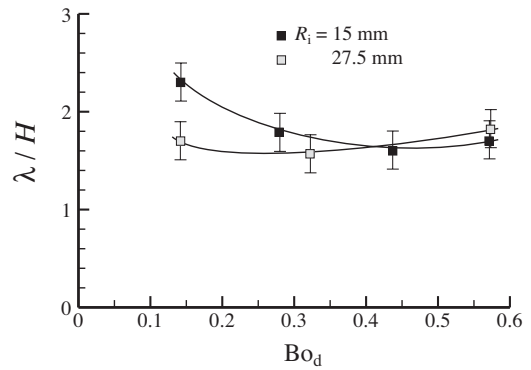


**Figure 6.** Dimensionless wavelength of hydrothermal wave.

### 3.2. Multicell

At  $H > 2.5$  mm, multicell patterns were dominant. Steady toroidal rolls first appeared as shown in figure 7(a).

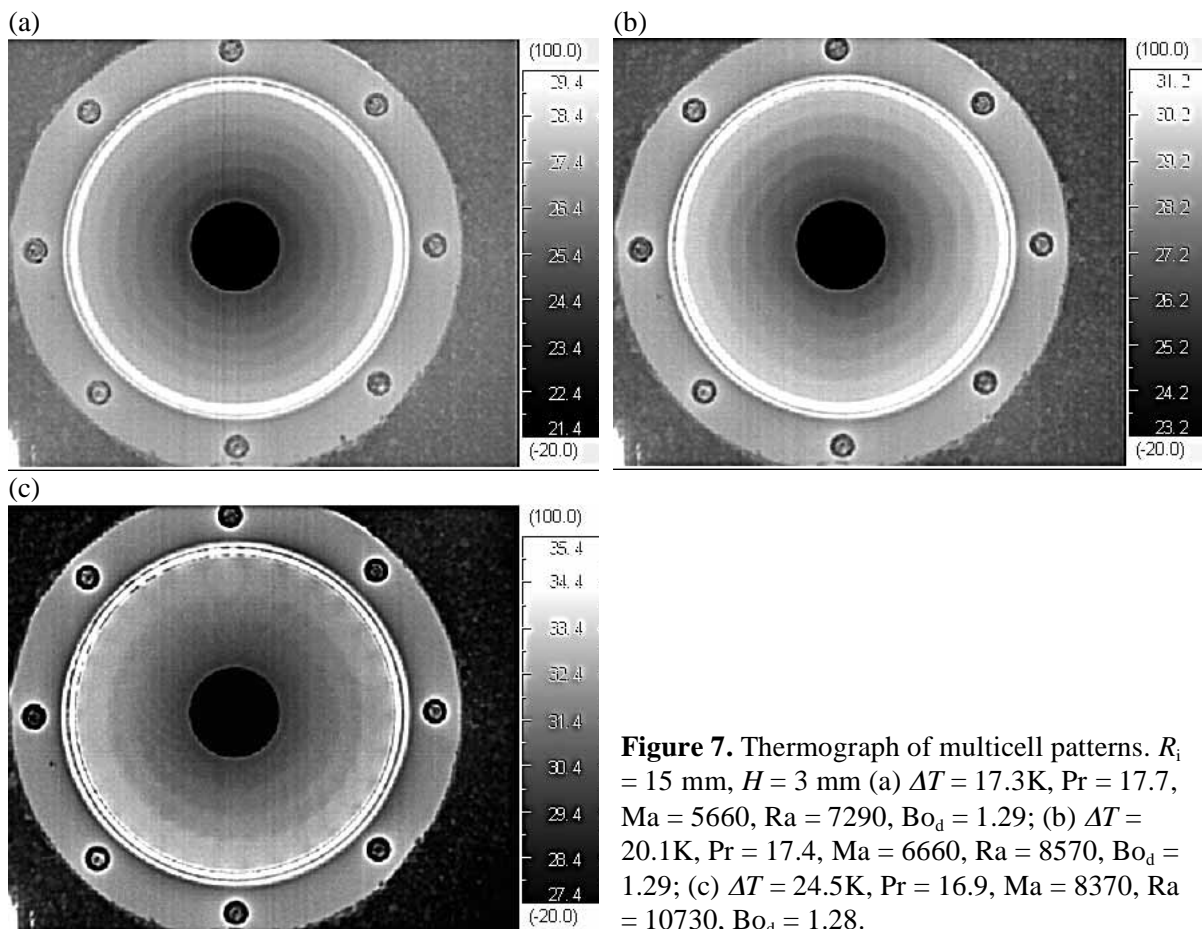


**Figure 7.** Thermograph of multicell patterns.  $R_i = 15$  mm,  $H = 3$  mm (a)  $\Delta T = 17.3$ K,  $Pr = 17.7$ ,  $Ma = 5660$ ,  $Ra = 7290$ ,  $Bo_d = 1.29$ ; (b)  $\Delta T = 20.1$ K,  $Pr = 17.4$ ,  $Ma = 6660$ ,  $Ra = 8570$ ,  $Bo_d = 1.29$ ; (c)  $\Delta T = 24.5$ K,  $Pr = 16.9$ ,  $Ma = 8370$ ,  $Ra = 10730$ ,  $Bo_d = 1.28$ .

As  $Ma$  was increased, the number of the toroidal rolls slightly decreased and began to rotate around the centre (figure 7 b). As  $Ma$  was further increased, unsteady, rotational longitudinal rolls appeared being superimposed on the toroidal rolls (figure 7 c). The patterns of this figure are those at  $H = 3$  mm, which corresponds to  $Bo_d = 1.3$ . Here, any hydrothermal wave does not appear.

At  $H = 2.8$  mm ( $Bo_d = 1.1$ ), on the other hand, the hydrothermal waves still appeared, and the waves and multicell coexisted as shown in figure 8.

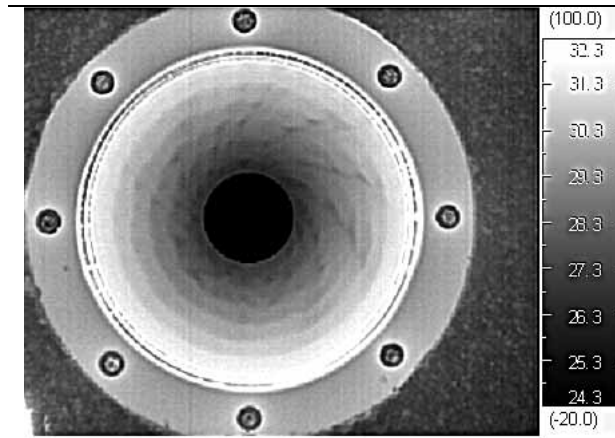


**Figure 8.** Thermograph of hydrothermal waves and multicell.  $R_i = 15$  mm,  $H = 2.8$  mm,  $\Delta T = 22.1$ K,  $Pr = 17.2$ ,  $Ma = 6480$ ,  $Ra = 7250$ ,  $Bo_d = 1.12$ .

### 3.3. Transition map

Figure 9 shows the transition map in the ( $Bo_d$ - $Ma$ ) plane to various unstable patterns observed in the present experiments. The scale of the Bond number  $Bo$  is added for reference. This result is for  $R_i = 15$  mm and it is substantially same as that for  $R_i = 27.5$  mm, although the latter is somewhat more stable.

These results show that an annular layer is more stable than a rectangular layer and a hydrothermal wave appears over a wide range of the dynamic Bond numbers.

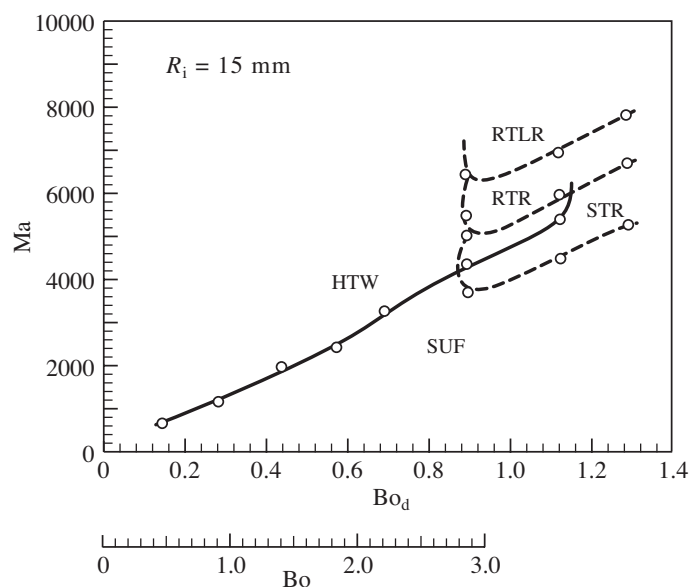


**Figure 9.** Transition map from steady unicellular flow (SUF) to hydrothermal waves (HTW), steady toroidal rolls (STR), rotating toroidal rolls (RTR), and rotating toroidal and longitudinal rolls (RTLRL).

#### 4. Conclusion

Experimental study of thermocapillary convection in shallow annular liquid layers was performed.

As  $Ma$  exceeded a critical value, hydrothermal waves were observed for thin liquid layers,  $H \leq 2.5$  mm ( $Bo_d \leq 0.9$ ). These waves are characterized by curved spoke patterns propagating in the azimuthal direction. For thicker layers,  $H > 2.5$  mm, multicell patterns were dominant. At low  $Ma$ , the multicell patterns were steady, toroidal rolls. As  $Ma$  was increased, the rolls began to rotate around the centre and unsteady longitudinal rolls appeared. For intermediate heights of layers,  $2.5 \leq H \leq 2.8$  mm ( $0.9 \leq Bo_d \leq 1.1$ ), hydrothermal waves and multicell coexisted.

#### References

- [1] Schatz M F and Neitzel G P 2001 *Annu. Rev. Fluid Mech.* **33** 93–129
- [2] Smith M K and Davis S H 1983 *J. Fluid Mech.* **132** 119–44
- [3] Riley R J and Neitzel G P 1998 *J. Fluid Mech.* **359** 143–64
- [4] Schwabe D, Möller U, Schneider J and Scharmann A 1992 *Phys. Fluids* **A4** 2368–81
- [5] Ezersky A B, Garcimartin A, Burguete J, Mancini H L and Pérez-García C 1993 *Phys. Rev. E* **47** 1126–31
- [6] Smith M K and Davis S H 1983 *J. Fluid Mech.* **132** 145–62
- [7] Kamotani Y, Ostrach S and Masud J 2000 *Fluid Mech.* **410** 211–33
- [8] Schwabe D, Zebib A and Sim B 2003 *J. Fluid Mech.* **491** 239–58
- [9] Garnier N, Chiffaudel A and Daviaud F 2006 *Dynamics of Spatio-Temporal Cellular Structures Henri Bénard Centenary Review*, ed I Mutabazi et al (New York: Springer) pp 147–161